Soft Matter

PAPER

View Article Online
View Journal | View Issue

Cite this: *Soft Matter*, 2015, 11, 5447

Impact of galactosylceramides on the nanomechanical properties of lipid bilayer models: an AFM-force spectroscopy study†

Berta Gumí-Audenis,[abc] Fausto Sanz[abc] and Marina I. Giannotti*[abc]

Galactosylceramides (GalCer) are glycosphingolipids bound to a monosaccharide group, responsible for inducing extensive hydrogen bonds that yield their alignment and accumulation in the outer leaflet of the biological membrane together with cholesterol (Chol) in rafts. In this work, the influence of GalCer on the nanomechanical properties of supported lipid bilayers (SLBs) based on DPPC (1,2-dipalmitoyl-*sn*-glycero-3-phosphocholine) and DLPC (1,2-didodecanoyl-*sn*-glycero-3-phosphocoline) as model systems was assessed. Phosphatidylcholine (PC):GalCer SLBs were characterized by means of differential scanning calorimetry (DSC) and atomic force microscopy (AFM), in both imaging and force spectroscopy (AFM-FS) modes. Comparing both PC systems, we determined that the behaviour of SLB mixtures is governed by the PC phase-like state at the working temperature. While a phase segregated system is observed for DLPC:GalCer SLBs, GalCer are found to be dissolved in DPPC SLBs for GalCer contents up to 20 mol%. In both systems, the incorporation of GalCer intensifies the nanomechanical properties of SLBs. Interestingly, segregated domains of exceptionally high mechanical stability are formed in DLPC:GalCer SLBs. Finally, the role of 20 mol% Chol in GalCer organization and function in the membranes was assessed. Both PC model systems displayed phase segregation and remarkable nanomechanical stability when GalCer and Chol coexist in SLBs.

Received 22nd May 2015,
Accepted 2nd June 2015

DOI: 10.1039/c5sm01252j

www.rsc.org/softmatter

Introduction

Biological membranes are flexible self-sealing boundaries that confine the permeability barriers of cells and organelles, providing the means to compartmentalize functions. They are not only essential as a structural part of the cell, but they also supply a support matrix for all the proteins that are inserted on it.[1] Biological membranes mediate diverse biological processes, like cell recognition and signalling, ion transference, adhesion and fusion. Their physical properties directly affect these processes and are not always easy to evaluate.

Regarding the composition, cell membranes are complex systems that include different components. In addition to all the proteins and carbohydrates, lipids are the main component in terms of molar fraction. To coordinate its functions, the membrane is able to laterally segregate its constituents. This is the raft concept of membrane subcompartmentalization, in which lipid rafts are nanoscale assemblies of sphingolipids, cholesterol and proteins, with essential functions in membrane signalling and trafficking.[2]

Surface glycosphingolipids (GSLs) are important communication devices used by cells, as they function as receptors in signalling, microbial and cellular adhesion processes, and display immunological identity.[3,4] GSLs contain an oligosaccharide headgroup covalently linked to a hydrophobic ceramide to anchor to the membrane. GSLs and cholesterol (Chol) are key components of lipid rafts. It is believed that Chol plays an essential role in the mechanisms behind the receptor function of GSLs[5–8] by regulating the GSL accessibility through direct conformational tuning of the headgroup.

Cerebrosides are a family of GSLs, specifically composed of a double-tailed ceramide (Cer), which is bound to a monosaccharide, either galactose (galactosylceramides, GalCer) or glucose (glucosylceramide, GlcCer), by a glycosidic linkage through the primary hydroxyl. They are commonly found to be highly saturated in natural sources, including the presence of a 2-hydroxy acyl chain in approximately 40–60% of them.[9,10] GalCer are found primarily in neuronal tissues and are the major glycosphingolipids in the central nervous system. They are the largest single

[a] *Institute for Bioengineering of Catalonia (IBEC), Baldiri Reixac 10-12, Barcelona, 08028, Spain. E-mail: migiannotti@ub.edu*
[b] *Physical Chemistry Department, Universitat de Barcelona, Barcelona, 08028, Spain*
[c] *Networking Biomedical Research Center on Bioengineering, Biomaterials and Nanomedicine (CIBER-BBN), Madrid, 28029, Spain*

† Electronic supplementary information (ESI) available: Vesicle characterization and dynamic force spectroscopy (DFS) data: F_b maps and histograms for pure DPPC and DPPC : GalCer (80 : 20) SLBs at different loading rates. See DOI: 10.1039/c5sm01252j

component of the myelin sheath of nerves and seem, along with other molecules, to form part of the structural support of the myelin sheath.[11] Cerebrosides are also significantly found in epithelial cells of the small intestine and colon, and in the granular sheath of the skin epidermis.[12–14] GalCer are involved in a very wide range of biological activities such as cell–cell interaction, intracellular communication, cellular development, and antitumor/cytotoxic effects.[15] GalCer transition temperature (T_m) is well above the physiological body temperature due to the extensive hydrogen bonding capability by lateral interaction between the saccharide headgroup and the hydroxy and amide groups of the sphingosine base of the ceramide part.[16,17] Accordingly, GalCer are aligned in a compact manner and they tend to be accumulated in the outer leaflet of the membrane together with cholesterol in rafts.[10,14]

Due to the chemical diversity of cell membranes, model bilayer systems, like supported lipid bilayers (SLBs), are very manageable platforms to investigate biological processes that occur at the cellular or subcellular level. Techniques with nanometric resolution like atomic force microscopy (AFM),[18–20] AFM-based force spectroscopy (AFM-FS)[21,22] and force clamp (AFM-FC)[23] are essential to probe local properties of lipid bilayers at the nanometre scale with a high spatial range sensitivity and versatility. An advantage of AFM is the possibility of controlling the environmental conditions, in such a manner that membrane-confined areas can be explored in liquid media and regulated temperature. By means of AFM-FS, it has been well founded that the maximum vertical force an SLB is able to stand before braking, the so-called breakthrough force F_b, is directly related to the lateral interactions between lipid molecules.[24] F_b appears as a discontinuity in the approaching force–distance curve (Fig. 1D) when the AFM tip breaks through the bilayer. Variations in the chemical structure of the phospholipid molecules[25] and in the physicochemical environment[26–29] cause changes in the F_b value, which is consequently considered as the fingerprint of the mechanical stability of a determined lipid membrane in a specific environment. In multicomponent systems, the F_b value can be directly associated with the bilayer composition of homogeneous systems or phase-segregated domains. AFM-FS contributes to clarify the nature of each phase observed in AFM topographical images.[30–35]

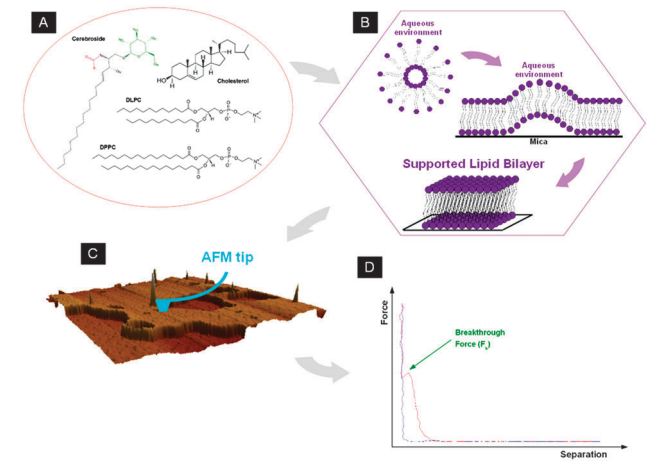

Fig. 1 (A) Chemical structures of cerebroside, cholesterol, DLPC and DPPC. (B) Diagram describing the supported lipid bilayer (SLB) preparation process by vesicle fusion. (C) SLB AFM topographical image (3D representation). (D) AFM-FS representative force–distance curve (approach: red; retrace: blue) showing the discontinuity associated with the bilayer failure (breakthrough force, F_b).

Although there are several studies on the GalCer domain formation in ternary mixtures together with Chol by means of AFM imaging,[10,14,36,37] no investigations of the influence of GalCer on the nanomechanical properties of gel and liquid-like systems have been reported. In this work we explore the influence of GalCer on the topography and mechanical stability of model lipid membranes. We use gel-like and liquid-like saturated phosphatidylcholine (PC) model SLBs, DPPC (1,2-dipalmitoyl-*sn-glycero*-3-phosphocholine) and DLPC (1,2-didodecanoyl-*sn-glycero*-3-phosphocoline). We follow by AFM imaging and AFM-FS the phase behaviour and nanomechanical properties of the SLBs, when up to 20 mol% GalCer are incorporated. As Chol is known to play an essential role in GSL organization and function in the membrane, we also evaluate the PC:GalCer SLBs when a specific amount of Chol (20 mol%) is introduced.

Experimental

Materials

1,2-Dipalmitoyl-*sn-glycero*-3-phosphocholine (DPPC), 1,2-dilauroyl-*sn-glycero*-3-phosphocoline (DLPC) and cholesterol (Chol) were purchased from Sigma-Aldrich (St. Louis, MO) and cerebrosides (ceramide beta-D-galactose, GalCer, from bovine spinal cord containing both hydroxy and non-hydroxy fatty acid side chains) from Matreya LLC (Pleasant Gap, PA). Chemical structures are shown in Fig. 1A. All of them were used without further purification. Chloroform was purchased from Aldrich (Aldrich, Steinheim, Germany) and methanol from SDS (Carlo Ebra, Milano, Italy). All experiments were performed in buffer solution of 150 mM NaCl, 20 mM $MgCl_2$, 20 mM Hepes (pH 7.4) prepared with ultrapure water (Milli-Q reverse osmosis system, 18.2 mΩ cm resistivity) and filtered before use using an inorganic membrane filter (0.22 μm pore size, Whatman International Ltd, England, UK).

Sample preparation

Liposome suspensions. DPPC, DLPC, Chol and GalCer were individually dissolved in a chloroform : methanol (3 : 1) mixture to give a final concentration of 3 mM. Aliquots of phospholipid solutions were mixed and poured into a falcon tube to obtain different compositions. Next, the solvent was evaporated to dryness under nitrogen flow in order to achieve a thin film on the walls of the tube. Afterwards, the dried phospholipid films were hydrated with buffer solution, previously heated above the transition temperature (T_m) of the lipid, until a final total concentration of 0.25–0.35 mM for SLBs and 7 mM for DSC experiments. The falcon tubes were then subjected to cycles of vortex mixing (1 min) and heating (20 s) to *ca.* 60 °C. The vesicle suspensions were placed in an ultrasound bath for 30 min to finally obtain mainly small unilamellar vesicles (SUVs)[38–41]

(DLS mean size distribution of vesicles containing GalCer are shown as examples in Fig. S1, ESI†).

Supported lipid bilayers (SLBs). SLBs were obtained by the commonly used SUV fusion method.[41] The lipid compositions of SUVs and the resultant SLBs are thought to be identical based on the phase separation observed in both membrane systems. Circular mica surfaces (Ted Pella, Redding, CA) were used as SLB substrates for AFM experiments. Before their use, mica surfaces were glued onto Teflon discs using epoxy-based mounting glue. In order to obtain SLBs, 100 μL of SUV suspension were deposited onto freshly cleaved mica and heated for 10–20 min at a temperature above the T_m of the lipid mixture (approximately T_m + 15 °C). After that, the samples were rinsed several times with buffer solution to avoid unfused vesicles, but were always kept hydrated on the mica substrates. The SLB preparation process is schematized in Fig. 1B. During the sample preparation procedure, phospholipid-containing solutions were always protected from light.

Differential scanning calorimetry (DSC)

DSC measurements were performed using a MicroCal VP-DSC (MicroCal, Northampton, MA). Approximately 600 μL of liposome suspensions (7 mM) were placed in the sample cell and the same volume of buffer solution was used as reference. With a 0.5 °C min^{-1} heating and cooling rate, the measurements were performed in the temperature range of 25 to 70 °C.

AFM imaging and force spectroscopy

AFM images and force spectroscopy (AFM-FS) measurements were performed using a MFP-3D atomic force microscope (Asylum Research, Santa Barbara, CA) using V-shaped Si_3N_4 cantilevers with sharp silicon tips and having a nominal spring constant of 0.35 N m^{-1} (SNL, Bruker AFM Probes, Camarillo, CA). After having measured the sensitivity of the piezo (V m^{-1}), the cantilever spring constants were individually calibrated by using the equipartition theorem (thermal noise routine).[42]

AFM images were acquired in both contact and AC modes at room temperature under liquid conditions (buffer solution). After imaging an interesting area, force–distance curves (Fig. 1D) were recorded by approaching and retracting the cantilever tip to the sample at constant velocity (1 μm s^{-1} was used, unless specifically stated, like in the dynamic force spectroscopy (DFS) experiments). Force curves were acquired in the force map mode, using an array of 32 × 32 (24 × 24 in the DFS experiments) points over a range of areas from 2 × 2 to 10 × 10 $μm^2$, depending on the observed phospholipid domain sizes in the scanned region.

Results and discussion

Gel-liquid phase transition on DPPC–GalCer vesicles: a DSC study

Following temperature increase, DPPC vesicles undergo a sharp phase transition at 41.6 °C, as displayed in the DSC thermograms shown in Fig. 2, from a solid-ordered or gel phase (s_o or $L_β$) to a liquid-disordered or liquid-crystalline phase (l_d or $L_α$).[31,43] Besides, a pretransition assigned to the change from a crystalline gel phase to a rippled gel phase ($P_β$) is observed at 34.7 °C. The order–disorder phase transition of GalCer vesicles occurs at considerably high temperature values, as a result of the hydrogen bonding capability of the saccharide headgroup and of the amide and hydroxy groups in the ceramide.[16,17] It has been reported that GalCer T_m is essentially independent of the acyl chain length, although the presence of a 2-OH group in the sequence lowers the temperature value.[10] GalCer used in this work is from a natural source (bovine) and contains both hydroxy and non-hydroxy fatty acid chains, displaying a relatively broad transition between 55 and 65 °C, with a maximum at 60.1 °C, as shown in Fig. 2.

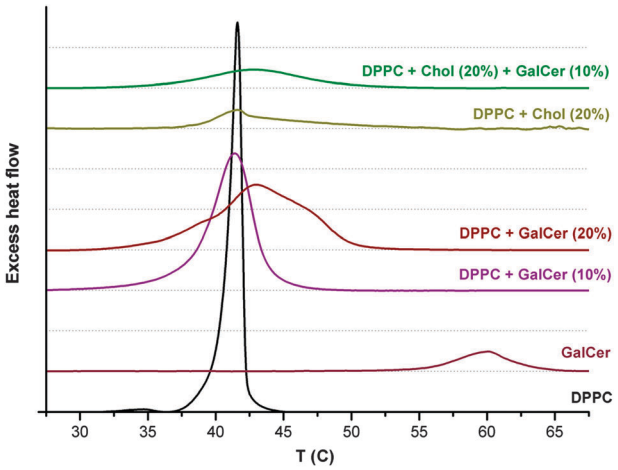

Fig. 2 DSC thermograms of lipid vesicles (7 mM): DPPC; GalCer; DPPC : GalCer (90 : 10 and 80 : 20 molar ratio); DPPC : Chol (80 : 20 molar ratio); and DPPC : Chol : GalCer (70 : 20 : 10 molar ratio). All suspensions were in 150 mM NaCl, 20 mM $MgCl_2$, and 20 mM Hepes (pH 7.4).

Upon addition of 10 mol% GalCer to the DPPC bilayer, a slight decrease in the main DPPC transition temperature to 41.4 °C is observed, whereas the phospholipid pretransition is no longer detected. Moreover, an increase of the transition peak width and asymmetry is observed. This could be associated with the coexistence of more than one phase with similar T_m or with the dissolution of GalCer in the DPPC bilayer, since no peak is detected in the temperature range of pure GalCer main transition. When increasing the GalCer content up to 20 mol%, the main transition of DPPC:GalCer vesicles occurs at a higher temperature, 43.0 °C, with two shoulders suggesting the formation of different domains on the lipid bilayer.

The incorporation of Chol into DPPC bilayers has been extensively studied in a previous work.[31] For Chol molar fractions higher than 10 mol%, Chol-rich and DPPC-rich phases coexist in the DPPC:Chol system. This occurs for compositions up to around 40 mol% of Chol, displaying thermograms where a sharp peak is assigned to the main transition of the DPPC-rich phase and a broader one corresponds to the melting of Chol-rich domains. As displayed in Fig. 2, we observe for DPPC : Chol (80 : 20 molar ratio) a broad transition that corresponds to the superimposition of a broader transition and a sharper one,

close to the one of pure DPPC. For the ternary system DPPC : Chol : GalCer (70 : 20 : 10 molar ratio), a very broad transition is observed at around 42.9 °C (Fig. 2). Again, no transition at temperatures corresponding to pure GalCer is detected.

AFM topography and nanomechanical stability of DPPC:GalCer model membranes

To evaluate the influence of GalCer on the DPPC bilayers, SLBs with molar fractions of GalCer up to 20% were imaged and characterized. As displayed in the AFM topography and profile shown in Fig. 3, DPPC extends onto the mica surface to form bilayer patches of about 4.5 nm thickness. For DPPC:GalCer SLBs with 10 mol% GalCer, no separated domains were observed, suggesting that GalCer are dissolved in the DPPC bilayer. However, in few regions it is possible to visualize some fissure-like features of about 300 pm depth in the topography that could be associated with certain extent of phase segregation. A similar scenario is observed when the GalCer content is increased to 20 mol%. Although there is no clear phase segregation in the form of domains, the SLB patches display certain heterogeneities in the form of fissure-like features with a depth of approximately 500 pm. These results are in agreement with the DSC predictions. However, it is important to keep in mind that the presence of a hard substrate may influence the lipid ordering and the inter-leaflet coupling[26] compared to the vesicle suspension tested in the DSC experiments.

To assess the influence of GalCer on the nanomechanical stability of DPPC systems, AFM-FS was performed to determine the maximum force the bilayer is able to withstand before failure, that is the breakthrough force F_b value (see Fig. 1D). A series of force–distance curves were performed over a previously imaged SLB region and F_b maps were built, which directly correlate with the topographical images (Fig. 3). A distribution of the recorded F_b values was fitted with a Gaussian model to determine the mean F_b value of the bilayer.

As displayed in Fig. 3, for DPPC:GalCer systems no clear separated domains can be identified in the F_b maps, and the F_b histograms display unimodal distributions. Nevertheless, the F_b distributions become wider and slightly asymmetric when increasing the GalCer content, especially for 20 mol%, which may be associated with a certain heterogeneity degree, as suggested from the observed topography and thermograms. The incorporation of GalCer into DPPC SLBs clearly increases the mechanical stability of the bilayers, as the F_b increases from 11.1 ± 0.9 nN for pure DPPC to 13.0 ± 1.2 nN for 10 mol% GalCer, and 21.2 ± 2.7 nN for 20 mol% GalCer (see Fig. 5a).

AFM topography and nanomechanical stability of DLPC:GalCer model membranes

To evaluate the effect of GalCer on the lateral order of liquid-like state SLBs, GalCer were incorporated into DLPC, a saturated phosphatidylcholine with 12-carbon chains instead of 16 (DPPC), and with a main transition temperature well below room temperature (T_m = −2 °C).

As observed in Fig. 4, DLPC tends to completely cover the mica surface due to its liquid-like state (l_d) at room temperature. Resulting from this liquid-phase behaviour, the bilayer thickness observed by AC mode AFM imaging for pure DLPC is *ca.* 2 nm. Upon incorporation of GalCer into the bilayer, segregation into different domains is observed for both 10 and 20mol% GalCer (Fig. 4). The segregated domains are seen as higher features in the topographical images (about 1.5 nm higher than the continuous phase).

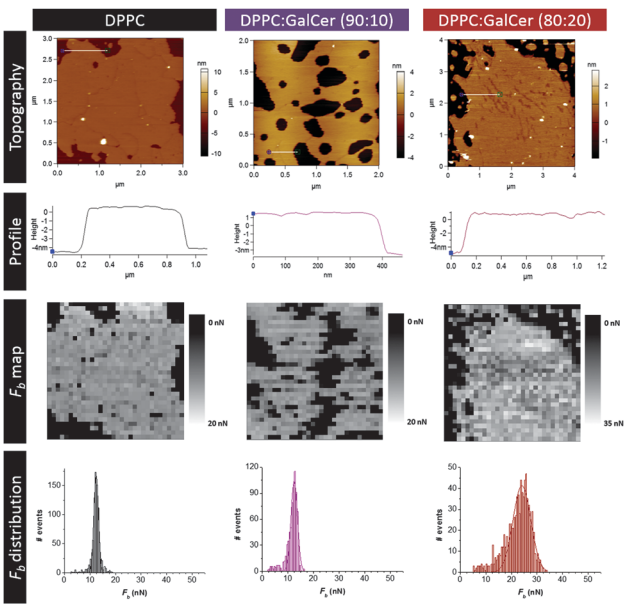

Fig. 3 AFM AC mode topographical images and profiles, with their corresponding AFM-FS results: F_b maps and F_b distributions for DPPC and DPPC : GalCer (90 : 10 and 80 : 20 molar ratio) SLBs deposited on mica in 150 mM NaCl, 20 mM $MgCl_2$, and 20 mM Hepes (pH 7.4).

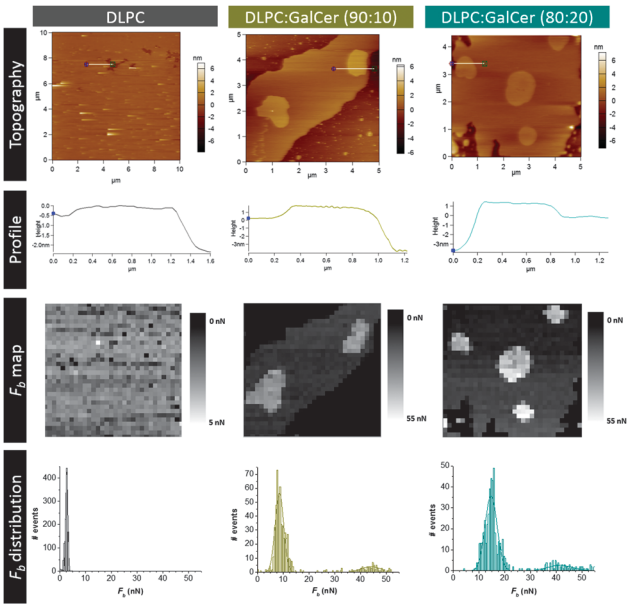

Fig. 4 AFM AC mode topographical images and profiles, with their corresponding AFM-FS results: F_b maps and F_b distributions for DLPC and DLPC : GalCer (90 : 10 and 80 : 20 molar ratio) SLBs deposited on mica in 150 mM NaCl, 20 mM $MgCl_2$, and 20 mM Hepes (pH 7.4).

Besides, the continuous phase is about 1 nm thicker than pure DLPC bilayers, the result that could be associated with the incorporation of partial glycosphingolipids into this phase. The higher domains display a similar thickness to the ones observed for gel-like DPPC bilayers, which suggests the coexistence of liquid and gel-like phases. It has been reported that in DLPC:GalCer SLBs formed by vesicle fusion, the GalCer domains display transbilayer asymmetry, with a difference in height between domains of *ca.* 1 nm, as opposed to height differences of 1.75 nm for symmetric domains in SLBs obtained through Langmuir–Blodget deposition, when measured from contact mode AFM.[14] In our case, the 1.5 nm difference obtained between domains may correspond to asymmetric bilayers, but the different compressibility properties of liquid and gel-like phases calculated from AC mode AFM images may lead to overestimated values.

As expected for a lipid bilayer in the l_d phase at room temperature, the bilayer failure process for DLPC SLBs occurs at significantly low F_b values, 2.7 ± 0.4 nN (Fig. 4 and 5b). When 10 and 20 mol% GalCer are incorporated into DLPC bilayers, two different populations are clearly distinguished in the F_b distributions, with mean values of 7.6 ± 1.0 and 43.6 ± 4.6 nN for 10 mol%, and 14.7 ± 2.3 and 41.5 ± 5.0 nN for 20 mol%, that correspond to the different phases observed in the AFM images (Fig. 4). According to the topography, the lower value is associated with the continuous phase, the DLPC-rich phase, whereas the higher F_b corresponds to the thicker domains, richer in GalCer. This GalCer-rich phase seems to be already saturated for the DLPC : GalCer 90 : 10 SLB, as for the DLPC : GalCer 80 : 20 SLB these domains display similar properties and very high F_b values, mainly due to the well-known capacity of GSLs to form strong hydrogen bonding interactions. The mechanical stability of the continuous phase (DLPC-rich phase) increases linearly with the general GalCer content of the bilayer, arriving to F_b values of the order of a gel-like SLB for DLPC : GalCer (80 : 20) (Fig. 5b).

Comparing both model systems (DPPC and DLPC), significant differences in the topographical images as well as in the mechanical stability are observed when adding a GalCer content up to 20 mol%. Hence, the phospholipid state at the working temperature is an essential parameter which governs the general behaviour of the SLB mixtures, although it is known that the structure and properties of GalCer-rich domains observed in liquid-like phospholipids are regulated also by the variation in the unsaturation degree and the chain length.[37] In general, no clear separated domains are observed in DPPC systems, whereas in DLPC, GalCer induces a phase separation in the bilayers. Both in DPPC and DLPC bilayers, the incorporation of GalCer up to 20 mol% provokes an increase in the F_b value (Fig. 5).

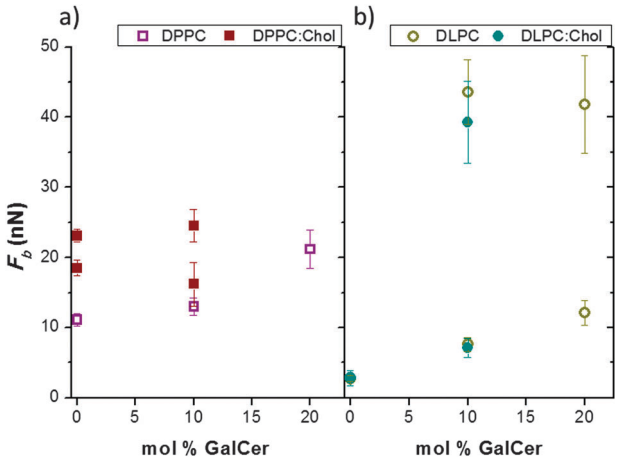

Fig. 5 Mean F_b values of: (a) DPPC and DPPC:Chol (20 mol% Chol) and (b) DLPC and DLPC:Chol (20 mol% Chol) SLBs in 150 mM NaCl, 20 mM $MgCl_2$, and 20 mM Hepes (pH 7.4) as a function of the GalCer content.

Influence of Chol in the GalCer distribution on DPPC and DLPC model SLBs

In view of the importance of the interplay between GSLs and Chol to tune GSL functions as membrane receptors and communicators, we evaluated the influence of Chol on the distribution of cerebrosides in the membrane and assessed its effect on the SLB mechanical properties. For this, a specific content of Chol was incorporated into binary mixtures composed of phospholipids (DPPC or DLPC) and GalCer. The resultant bilayers were imaged and characterized with AFM and force spectroscopy, as done with the previous binary systems.

As already discussed, a DPPC bilayer containing 10 mol% of GalCer showed no clear separated domains and a unimodal F_b distribution (13.0 ± 1.2 nN) (Fig. 3), suggesting the dissolution of GalCer into DPPC bilayers. Prior to the three-component mixture assessment, a DPPC bilayer with the addition of 20 mol% Chol was evaluated. When 20 mol% Chol is incorporated into the DPPC bilayers, the coexistence of two different phases with approximately 300 pm height difference occurs, as observed in the topography image corresponding to this system shown in Fig. 6. As reported earlier,[31] the higher domains are associated with a Chol-rich phase and the lower continuous domain corresponds to a DPPC-rich phase, the results that are in agreement with those obtained in the DSC thermograms (see Fig. 2). In accordance, this system shows a bimodal distribution of F_b when evaluated by force spectroscopy, with mean values of 18.5 ± 1.1 and 23.1 ± 0.9 nN, associated with the DPPC-rich and Chol-rich phases, respectively (Fig. 6 and 5a).

Part of the DPPC content was then replaced by GalCer and SLBs of DPPC : Chol : GalCer (70 : 20 : 10 molar ratio) were prepared and evaluated. AFM topographical and force spectroscopy results are shown in Fig. 6. Regarding the topographical image, this mixture displays phase segregation with a difference in height of approximately 500 pm between domains. Taking into account the domain formation in the DPPC : Chol (80 : 20 molar ratio) system and the lack of domains in DPPC bilayers containing 10 mol% GalCer, the thicker domains may correspond to Chol-rich phases, whereas the thinner ones may be associated with Chol-poor phases.

Accordingly, the nanomechanical characterization of the DPPC:Chol:GalCer blend results in a bimodal F_b histogram, with mean values of 16.2 ± 3.1 and 24.5 ± 2.3 nN for each of the phases, as seen in the F_b map (Fig. 6). These values are similar to the ones obtained with the DPPC:Chol system, which raises

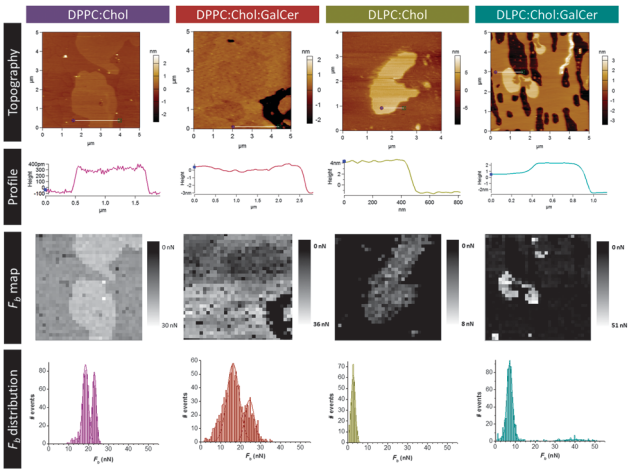

Fig. 6 AFM AC mode topographical images and profiles with their corresponding F_b maps and F_b distributions of DPPC : Chol (80 : 20 molar ratio), DPPC : Chol : GalCer (70 : 20 : 10 molar ratio), DLPC : Chol (80 : 20 molar ratio) and DLPC : Chol : GalCer (70 : 20 : 10 molar ratio) SLBs deposited on mica in 150 mM NaCl, 20 mM $MgCl_2$, and 20 mM Hepes (pH 7.4).

the possibility of having GalCer dissolved in both Chol-rich and Chol-poor domains. Still, a slight increase of the mechanical stability of the Chol-rich domains might be associated with a preferential distribution of GalCer towards the Chol-rich phase.

Conversely, Chol is generally totally dissolved in liquid-like phospholipid bilayers such as DOPC, giving a homogeneous F_b distribution when pierced by AFM.[31] The same behaviour was observed here when 20 mol% Chol was incorporated into DLPC bilayers, as displayed in Fig. 6, where a membrane patch of homogeneous topography and F_b distribution with a mean value of 2.8 ± 1.0 nN is shown.

As previously discussed, phase segregated SLBs were clearly visualized in DLPC:GalCer bilayers, where GalCer seems to be the main component of the higher domains, but also appears to affect the DLPC-rich region (lower domains), leading to an increase in F_b (Fig. 4 and 5b). When Chol is introduced into the system to obtain SLBs of DLPC : Chol : GalCer (70 : 20 : 10 molar ratio), the system shows two separated domains (Fig. 6), with *ca.* 1.2 nm height difference. As can be seen in the F_b distribution of Fig. 6 and in Fig. 5b, the mean F_b values for each domain are 7.1 ± 1.4 and 39.3 ± 5.8 nN. Both phases display considerably higher nanomechanical stability than the DLPC : Chol (80 : 20 molar ratio) SLBs, although similar to DLPC : GalCer (90 : 10) SLBs. Hence, for low GalCer contents, 20 mol% Chol barely affects pure DLPC bilayers and the GalCer distribution on them.

SLB rupture activation energy of the DPPC model system: the influence of GalCer

Mechanical rupture of lipid bilayers is of thermal-fluctuation nature and the application of an external force facilitates and directs the destructive action of the thermal fluctuations. The penetration of the cantilever tip into the lipid bilayer has been modelled and widely conceived as a two-state activated process[44] with an associated energy barrier that follows the Arrhenius law (eqn (1)). The probability for lipid bilayer rupture by thermal fluctuations is then proportional to the Boltzmann factor (k_B):

$$k(t) = A\mathrm{e}^{-\left(\frac{\Delta E(t)}{k_B T}\right)} \quad (1)$$

where the pre-exponential factor A is defined as the frequency at which the AFM tip attempts to penetrate the bilayer, ΔE is the activation energy required for the formation of a hole in the bilayer that is large enough to initiate rupture and lead the tip breakthrough and T is the absolute temperature.

The thermomechanically activated nature of the bilayer rupture kinetics gives rise to a loading-rate (ν) dependence, which allows the calculation of the activation energy of the bilayer rupture in the absence of an external force (ΔE_0). As the bilayer rupture and breakthrough of the AFM tip are usually represented in terms of force rather than in terms of time, and considering that the tip is moving at a constant velocity towards the sample, the load increases according to $F = K\nu t$. K is the spring constant of the cantilever and F is the force applied at time t. Using the relation between the force dependence of the activation energy ΔE and the force dependence of the loading rate proposed by Butt *et al.*,[44] the activation energy of the bilayer failure can be calculated (eqn (2)):

$$\Delta E(F_b) = -k_B T \ln\left[\left(\frac{0.693K}{A}\right)\frac{\mathrm{d}\nu}{\mathrm{d}F_b}\right] \quad (2)$$

In dynamic force spectroscopy (DFS) experiments on indentation of SLBs, it has been well established that the mean breakthrough force F_b increases linearly with the logarithm of the loading rate[34,44–46] (eqn (3)). Combining eqn (2) and (3) into eqn (4) and extrapolating this relation to zero mean breakthrough force (F_b = 0) we calculate the ΔE_0.

$$F_b = a + b\log\nu \quad (3)$$

$$\begin{aligned}\Delta E(F_b) &= -k_B T \ln\left(\frac{1.60K}{Ab}\nu\right)\\ &= k_B T\left[2.30\frac{a - F_b}{b} - \ln\left(\frac{1.60K}{Ab}\right)\right]\end{aligned} \quad (4)$$

We collected data by means of DFS at different loading rates (in the range between 0.5 and 6 μm s^{-1}) for pure DPPC and DPPC : GalCer (80 : 20 molar ratio) SLBs (Fig. S2 and S3, ESI† display the corresponding F_b maps and histograms). As shown in Fig. 7, the F_b mean values display a linear behaviour with the logarithm of the loading rate, for both SLB systems. From the linear fitting we obtain a and b (eqn (3)), when F_b and ν are expressed in N and m seg^{-1}, respectively, and calculate ΔE_0 using eqn (4) (with F_b = 0, K = 0.35 N m^{-1} and A = 8600 Hz). The resulting values are very similar for both systems: 9.9 ± 2.7k_BT for pure DPPC and 9.1 ± 1.1k_BT for DPPC : GalCer (80 : 20). These values are in the range of the reported ones.[23,45]

The loading rate is the rate at which the applied force increases from F to F + ΔF, determining how fast the force on the SLB increases. The observed dependence of the F_b with the loading rate indicates that the higher the loading rate, the less time (less chances)

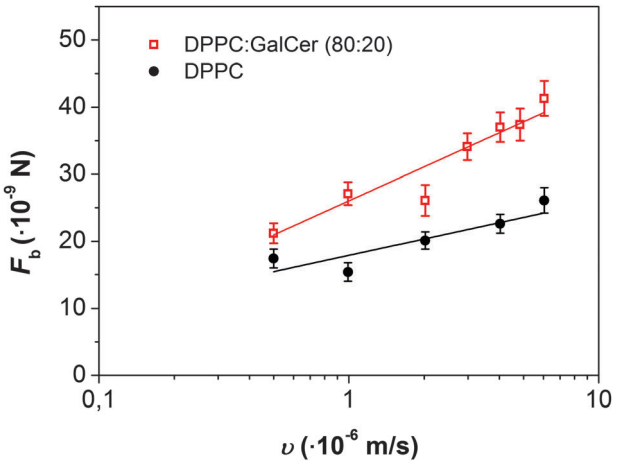

Fig. 7 Dynamic F_b spectra: dependence of the mean F_b on the loading rate for DPPC and DPPC : GalCer (80 : 20 molar ratio) SLBs deposited on mica in 150 mM NaCl, 20 mM $MgCl_2$, and 20 mM Hepes (pH 7.4).

for the bilayer to rupture in an interval of force increase (ΔF). This is a general behaviour observed for AFM tip indentation on SLBs. Although no differences in the activation energy values are observed for the two systems (DPPC and DPPC:GalCer), the rate at which F_b increases with the logarithm of the tip velocity is higher for the DPPC:GalCer than for DPPC SLBs. This suggests that GalCer, due to its extensive hydrogen bonding capability, directly affect the thermal fluctuations of the DPPC bilayer, yielding more chance for the SLB to remain intact than for pure DPPC, considering the same interval of force increase.

Conclusions

Model systems based on DPPC and DLPC SLBs incorporating 10 and 20 mol% GalCer were studied by means of DSC, AFM imaging and AFM-FS. The phospholipid state (gel-like, s_o, for DPPC, or liquid-like, l_d, for DLPC) at the working temperature is a defining parameter governing the behaviour of lipid bilayer mixtures. Upon the introduction of GalCer, phase segregation does not occur in DPPC SLBs, while separated domains are clearly manifested in DLPC SLBs. In general, amounts up to 20 mol%, GalCer provoke an increase in the nanomechanical stability for both systems. Interestingly, the segregated domains in DLPC:GalCer SLBs are of exceptionally high mechanical stability, while increasing amounts of GalCer confer characteristics typical of gel-like SLBs on the continuous DLPC-rich phase.

Chol appears to be determinant for the domain formation, GalCer distribution and enhanced nanomechanical properties of DPPC : Chol : GalCer (70 : 20 : 10) SLBs. On the other hand, for DLPC:Chol:GalCer SLBs, the phase behaviour and mechanical stability are dominated by the GalCer partial immiscibility, while Chol barely affects DLPC bilayers with low contents of GalCer.

By means of DFS, the lineal increment of the F_b with the logarithm of the loading rate was observed for DPPC and DPPC:GalCer SLBs. This effect is more pronounced (steeper slope) when GalCer are present in the SLB, due to their extensive hydrogen bonding capability. The activation energy of the bilayer failure in the absence of force calculated for both systems was in the range of the ones previously reported.

Acknowledgements

Financial support from Agència de Gestió d'Ajuts Universitaris i de Recerca (AGAUR) through 2014SGR-1251 is acknowledged. We are grateful to G. Oncins and J. Díaz (Nanometric Techniques Unit) and R. Barbas (Polymorphism and Calorimetry Unit) of the Scientific and Technical Center of the University of Barcelona (CCiTUB) for technical assistance.

References

1 W. Dowhan, *Annu. Rev. Biochem.*, 1997, **66**, 199–232.
2 D. Lingwood and K. Simons, *Science*, 2010, **327**, 46–50.
3 S.-i. Hakomori, *Biochim. Biophys. Acta, Gen. Subj.*, 2008, **1780**, 325.
4 R. Malhotra, *Biochem. Anal. Biochem.*, 2012, **1**, 1000108.
5 D. Lingwood, B. Binnington, T. Róg, I. Vattulainen, M. Grzybek, Ü. Coskun, C. A. Lingwood and K. Simons, *Nat. Chem. Biol.*, 2011, **7**, 260.
6 N. Yahi, A. Aulas and J. Fantini, *PLoS One*, 2010, **5**, e9079.
7 J. Fantini, N. Yahi and N. Garmy, *Front. Physiol.*, 2013, **4**, 120.
8 T. Róg and I. Vattulainen, *Chem. Phys. Lipids*, 2014, **184**, 82.
9 X. L. Han and H. Cheng, *J. Lipid Res.*, 2005, **46**, 163–175.
10 M. L. Longo and C. D. Blanchette, *Biochim. Biophys. Acta, Biomembr.*, 2010, **1798**, 1357–1367.
11 A. Huwiler, T. Kolter, J. Pfeilschifter and K. Sandhoff, *Biochim. Biophys. Acta, Mol. Cell Biol. Lipids*, 2000, **1485**, 63–99.
12 G. C. Hansson, *Biochim. Biophys. Acta*, 1983, **733**, 295–299.
13 G. M. Gray, I. A. King and H. J. Yardley, *J. Invest. Dermatol.*, 1978, **71**, 131–135.
14 C. D. Blanchette, W. C. Lin, T. V. Ratto and M. L. Longo, *Biophys. J.*, 2006, **90**, 4466–4478.
15 X. Zhou, L. Tang and Y. Liu, *Lipids*, 2009, **44**, 759–763.
16 J. M. Boggs, *Biochim. Biophys. Acta, Rev. Biomembr.*, 1987, **906**, 353.
17 P.-G. Nyholm, I. Pascher and S. Sundell, *Chem. Phys. Lipids*, 1990, **52**, 1.
18 S. Scheuring and Y. F. Dufrene, *Mol. Microbiol.*, 2010, **75**, 1327–1336.
19 M. R. Nussio, R. D. Lowe, N. H. Voelcker, B. S. Flavel, C. T. Gibson, M. J. Sykes, J. O. Miners and J. G. Shapter, *Soft Matter*, 2010, **6**, 2193–2199.
20 A. Alessandrini and P. Facci, *Soft Matter*, 2014, **10**, 7145–7164.
21 S. Garcia-Manyes and F. Sanz, *Biochim. Biophys. Acta, Biomembr.*, 2010, **1798**, 741.
22 L. Redondo-Morata, M. I. Giannotti and F. Sanz, in *Atomic Force Microscopy in Liquid*, ed. A. M. Baró and

R. G. Reifenberger, Wiley-VCH Verlag GmbH & Co. KGaA, Weinheim, Germany, 2012.
23 L. Redondo-Morata, M. I. Giannotti and F. Sanz, *Langmuir*, 2012, **28**, 6403–6410.
24 Y. F. Dufrêne, T. Boland, J. W. Schneider, W. R. Barger and G. U. Lee, *Faraday Discuss.*, 1999, **111**, 79.
25 S. Garcia-Manyes, L. Redondo-Morata, G. Oncins and F. Sanz, *J. Am. Chem. Soc.*, 2010, **132**, 12874–12886.
26 S. Garcia-Manyes, G. Oncins and F. Sanz, *Biophys. J.*, 2005, **89**, 4261–4274.
27 S. Garcia-Manyes, G. Oncins and F. Sanz, *Biophys. J.*, 2005, **89**, 1812–1826.
28 S. Garcia-Manyes, G. Oncins and F. Sanz, *Electrochim. Acta*, 2006, **51**, 5029–5036.
29 L. Redondo-Morata, M. I. Giannotti and F. Sanz, *Mol. Membr. Biol.*, 2014, **31**, 17–28.
30 L. Picas, M. T. Montero, A. Morros, M. E. Cabañas, B. Seantier, P.-E. Milhiet and J. Hernández-Borrell, *J. Phys. Chem. B*, 2009, **113**, 4648.
31 L. Redondo-Morata, M. I. Giannotti and F. Sanz, *Langmuir*, 2012, **28**, 12851–12860.
32 L. M. C. Lima, M. I. Giannotti, L. Redondo-Morata, M. L. C. Vale, E. F. Marques and F. Sanz, *Langmuir*, 2013, **29**, 9352–9361.
33 S. Zou and L. J. Johnston, *Curr. Opin. Colloid Interface Sci.*, 2010, **15**, 489–498.
34 R. M. A. Sullan, J. K. Li, C. Hao, G. C. Walker and S. Zou, *Biophys. J.*, 2010, **99**, 507.
35 F. Guyomarc'h, S. Zou, M. Chen, P.-E. Milhiet, C. Godefroy, V. Vié and C. Lopez, *Langmuir*, 2014, **30**, 6516.
36 W.-C. Lin, C. D. Blanchette and M. L. Longo, *Biophys. J.*, 2007, **92**, 2831.
37 C. D. Blanchette, W.-C. Lin, C. A. Orme, T. V. Ratto and M. L. Longo, *Biophys. J.*, 2008, **94**, 2691.
38 S. J. Attwood, Y. Choi and Z. Leonenko, *Int. J. Mol. Sci.*, 2013, **14**, 3514–3539.
39 L. Bagatolli and P. B. Sunil Kumar, *Soft Matter*, 2009, **5**, 3234.
40 D. M. Carter Ramirez, Y. A. Kim, R. Bittman and L. J. Johnston, *Soft Matter*, 2013, **9**, 4890.
41 M.-P. Mingeot-Leclercq, M. Deleu, R. Brasseur and Y. F. Dufrene, *Nat. Protoc.*, 2008, **3**, 1654.
42 R. Proksch, T. E. Schaffer, J. P. Cleveland, R. C. Callahan and M. B. Viani, *Nanotechnology*, 2004, **15**, 1344–1350.
43 D. Marsh, *Chem. Phys. Lipids*, 1991, **57**, 109–120.
44 H.-J. Butt and V. Franz, *Phys. Rev. E: Stat., Nonlinear, Soft Matter Phys.*, 2002, **66**, 031601.
45 S. Loi, G. Sun, V. Franz and H.-J. Butt, *Phys. Rev. E: Stat., Nonlinear, Soft Matter Phys.*, 2002, **66**, 031602.
46 V. Franz, S. Loi, H. Müller, E. Bamberg and H.-J. Butt, *Colloids Surf., B*, 2002, **23**, 191.

